HHS Public Access

Author manuscript

Appl Ergon. Author manuscript; available in PMC 2022 October 26.

Published in final edited form as:

Appl Ergon. 2020 November ; 89: 103187. doi:10.1016/j.apergo.2020.103187.

Measuring upper arm elevation using an inertial measurement unit: An exploration of sensor fusion algorithms and gyroscope models

Howard Chen[a,*], **Mark C. Schall Jr.**[b], **Nathan B. Fethke**[c]

[a]Department of Mechanical Engineering, Auburn University, AL, USA

[b]Department of Industrial and Systems Engineering, Auburn University, AL, USA

[c]Department of Occupational and Environmental Health, University of Iowa, Iowa City, IA, USA

Abstract

Many sensor fusion algorithms for analyzing human motion information collected with inertial measurement units have been reported in the scientific literature. Selecting which algorithm to use can be a challenge for ergonomists that may be unfamiliar with the strengths and limitations of the various options. In this paper, we describe fundamental differences among several algorithms, including differences in sensor fusion approach (e. g., complementary filter vs. Kalman Filter) and gyroscope error modeling (i.e., inclusion or exclusion of gyroscope bias). We then compare different sensor fusion algorithms considering the fundamentals discussed using laboratory-based measurements of upper arm elevation collected under three motion speeds. Results indicate peak displacement errors of <4.5° with a computationally efficient, non-proprietary complementary filter that did not account for gyroscope bias during each of the one-minute trials. Controlling for gyroscope bias reduced peak displacement errors to <3.0°. The complementary filters were comparable (<1° peak displacement difference) to the more complex Kalman filters.

Keywords

Inclinometer; Kalman filter; Complementary filter; Inertial measurement units; Inertial-based motion capture

1. Introduction

Inertial measurement units (IMUs) are appealing for capturing human motion in unconstrained environments due to their ability to reliably record information about worker kinematics across full working shifts with minimal worker obtrusion (Douphrate et al., 2012). As such, IMUs have been increasingly used by ergonomists and those in related fields to quantify human motion in the workplace (Schall et al., 2016a; Kersten and Fethke, 2019; Granzow et al., 2018). IMU-based motion measurements, however, are subject to a

*Corresponding author. hzc0074@auburn.edu (H. Chen).

Declaration of competing interest

The authors declare that there is no conflict of interest regarding the publication of this article.

variety of error sources, such as magnetic disturbances (Bachmann et al., 2004; Fan et al., 2017; Ligorio and Sabatini, 2016; Robert-Lachaine et al., 2017; de Vries et al., 2009) and high motion speeds (Chen et al., 2017; Ricci et al., 2016; Lebel et al., 2013). In general, three-dimensional (3D) full-body motion capture is possible under nominal conditions, but full-shift 3D motion capture in unconstrained environments may be unattainable based on current hardware capabilities (Robert-Lachaine et al., 2017; Chen et al., 2017).

Much of the biomechanics and ergonomics literature regarding IMUs entails validation and application of commercially available inertial-based motion capture systems (Lebel et al., 2013; Robert-Lachaine et al., 2016; Robert-Lachaine et al., 2019; Kim and Nussbaum, 2014; Lebel et al., 2015; Blair et al., 2018; Cloete and Scheffer, 2008; Godwin et al., 2009; Zhang et al., 2013; Sers et al., 2020). While these studies have thoroughly documented the inherent limitations of IMU-based motion capture systems, both IMU error magnitudes and characteristics can deviate substantially among sensor models and manufacturers (Lebel et al., 2013). Consequently, the error magnitudes reported in these studies have limited generalizability beyond a certain manufacturer and/or model of IMUs, and perhaps even software versions. The differences in error characteristics among the manufacturers may, in part, be attributed to differences in signal processing methods (Chen et al., 2017; Chang et al., 2016; Filippeschi et al., 2017; Miezal et al., 2016). For this reason, we advocate for the use of non-proprietary sensor fusion algorithms, given that known error characteristics and failure modes may be more advantageous to a practicing ergonomist than potential increases in accuracy that may come from a proprietary algorithm. To our knowledge, the literature describing various sensor fusion methods available for IMU-based motion capture has not been synthesized for practicing ergonomists.

In this paper, we review the fundamentals of IMU-based motion capture and discuss the differences among several sensor fusion algorithms for IMU-based motion capture. This synthesis of the literature provides readers information to consider when selecting a sensor fusion algorithm for occupational ergonomics applications. Additionally, we evaluate the accuracy of four different sensor fusion algorithms, consisting of differences in sensor fusion approach and gyroscope error model, using laboratory-based measurements of upper arm elevation and velocity under a variety of motion speeds during a controlled experiment.

2. Fundamentals of inertial-based motion capture

An IMU used for human motion capture contains a miniature gyroscope, accelerometer, and, sometimes, a magnetometer. The gyroscope measures angular velocities, which are subsequently integrated with respect to time to obtain orientation (Bergamini et al., 2014; Brodie et al., 2008). This is known as dead-reckoning. In theory, joint angles can be estimated by calculating the relative orientation between two gyroscopes attached to adjacent body segments. In practice, since orientation is obtained by integrating angular velocities with respect to time, errors associated with the angular velocities measured by the gyroscope are integrated as well, which then compound with time (Lebel et al., 2015). All gyroscopes, regardless of size and cost, exhibit this error characteristic, known as gyroscopic drift. The advantages of the gyroscopes used for IMU-based motion capture reside in their miniature size, low cost, and durability, rather than measurement accuracy.

Gyroscopic drift is eliminated by leveraging a sensor fusion algorithm to augment gyroscope measurements with information provided through additional sensors and assumptions about human motion. In general, the gyroscope-derived orientation measurements are augmented with information about sensor orientation with respect to both gravity (from an accelerometer) and magnetic north (from a magnetometer) (Bergamini et al., 2014; Yun et al., 2008; Valenti et al., 2015; Schiefer et al., 2014). This approach considers a time-invariant orientation under the assumption that the accelerometer is responding only to gravity and that the magnetometer is responding only to Earth's local magnetic field. The assumption that an accelerometer is responding only to gravity is violated under periods of motion, which can cause peak errors exceeding 25° in measurements of upper arm elevation with respect to gravity (Chen et al., 2018). The assumption of a homogeneous local magnetic field is violated when an IMU is placed within proximity of ferromagnetic objects and electronic devices, which can cause errors up to 180° (Bachmann et al., 2004; Ligorio and Sabatini, 2016). Thus, while combining accelerometer and magnetometer measurements with gyroscope measurements can eliminate the effects of gyroscopic drift, orientation may still be adversely affected by increased motion speeds and the presence of ferromagnetic disturbances (Chen et al., 2017).

The extent to which errors due to increased motion speeds and magnetic disturbances can be mitigated is ultimately bound by the quality of the gyroscope used; accelerometer and magnetometer measurements would not be needed with a "perfect" gyroscope. In the absence of such a gyroscope, the goal of a sensor fusion algorithm is to provide an estimate of orientation that is unaffected by gyroscopic drift as well as motion and magnetic disturbances.

Fig. 1 illustrates upper arm inclination (pitch) angles calculated using only accelerometer measurements and using a sensor fusion algorithm that combines accelerometer with gyroscope measurements. The absence of gyroscopic drift is indicated by the identical inclination angles calculated from the accelerometer and fused approaches during static periods, acknowledging that slight offsets will sometimes exist as an artifact of the sensor fusion process. However, the accelerometer-only measurements deviate relative to the fused measurements during periods of motion, especially those with faster motion speeds (e.g. seconds 550 to 600). During these periods, fused solutions produced more accurate measurements than accelerometer-only measurements due to the mitigation of non-gravitational acceleration.

Fig. 2 illustrates how measurements about gravity (heading) calculated using accelerometer and gyroscope information differ with and without the inclusion of magnetometer information in the fusion algorithm. The time-varying offset between heading measurements calculated with and without magnetometer information is characteristic of gyroscopic drift. During the first 75 s of the trial, the deviations were minimal (<3° degrees), but exceeded 60° 14 min (940 s) into the trial.

Many approaches have been described for calculating orientation using combinations of gyroscope, accelerometer, and magnetometer measurements. The differentiating factors among the various sensor fusion algorithms for IMU-based motion capture entail differences

in (i) sensor error models, (ii) sensor fusion approaches, and (iii) mechanisms to mitigate errors related to motion and magnetic disturbances.

2.1. Sensor error model considerations

The sensor error model considers the difference between the sensor measurement and its nominal value. For gyroscopes, accelerometers, and magnetometers, this difference can be explained through scaling, bias (offset), and presence of uncorrelated white Gaussian noise (Sabatini, 2006). For magnetometers, scaling and bias are typically pre-determined using a calibration procedure performed by the user to account for the presence of static magnetic disturbances (e.g. metal screws used to secure a case around the IMU) (Kok and Schön, 2016; Gebre-Egziabher et al., 2006). The scaling factors for the accelerometer and gyroscope are assumed to be pre-determined at the time of manufacture. The accelerometer bias is typically considered negligible when the accelerometer is used to measure the direction of the gravity vector. Consequently, accelerometer white noise, magnetometer white noise, gyroscope white noise, and gyroscope bias are considered the only error sources in the model. Some sensor fusion algorithms (e.g. (Ligorio and Sabatini, 2016; Madgwick et al., 2011; Wu et al., 2016; Yun and Bachmann, 2006)) do not account for changes in gyroscope bias to simplify filter parameters and achieve faster computation times.

2.2. Sensor fusion approach

The purpose of any sensor fusion algorithm is to attenuate random and systematic measurement errors by combining information from multiple sources (Plamondon et al., 2007). Perhaps the simplest approach, both conceptually and computationally, is the complementary filter, which leverages the high-frequency components of gyroscope measurements with the low-frequency components of accelerometer and magnetometer measurements (Madgwick et al., 2011; Luinge and Veltink, 2005). The Kalman Filter is also a common sensor fusion approach. A Kalman Filter is designed using a pre-defined statistical model under an assumption that measurement error is both Gaussian and stochastic (Sabatini, 2011).

Advantages of complementary filters include computational efficiency and simple tuning (Valenti et al., 2015). This approach, therefore, is useful for running on a small microprocessor in real-time or when post-processing large data files collected over long durations. However, the Kalman Filter provides (i) theoretically more accurate measurements given the same input information as the complementary filter and (ii) increased flexibility to incorporate extensions to improve measurement accuracy (e.g. human kinematic models), but at the expense of increased filter complexity and computational costs. Common Kalman Filter variations include Extended Kalman Filters (Sabatini, 2006; Yun and Bachmann, 2006; Brigante et al., 2011), Linear Kalman Filters (Ligorio and Sabatini, 2015a; Valenti et al., 2016), Unscented Kalman Filters (Kraft, 2003; LaViola, 2003), and Indirect Kalman Filters (Chang et al., 2016; Luinge and Veltink, 2005; Kortier et al., 2014; Nez et al., 2018; Del Rosario et al., 2018). Each variation has been used to combine gyroscope, accelerometer, and magnetometer measurements to calculate spatial orientation, of which the Extended Kalman Filter is most commonly used in IMU-based applications (Sabatini, 2011).

2.2.1. Mechanisms to mitigate motion disturbances—Many sensor fusion implementations contain a mechanism to account for non-gravitational acceleration. Since fast (e.g. 100°/s) human motion is unlikely to be sustained, non-gravitational acceleration can be modeled as a time-varying decay in linear acceleration (Ligorio and Sabatini, 2015b; Roetenberg et al., 2005; Lee et al., 2012) or angular velocity (Yun and Bachmann, 2006). Another approach is to discard or de-weight accelerometer measurements when the acceleration vector sum exceeds that of gravity (Sabatini, 2006; Sun et al., 2013), and rely on gyroscope dead-reckoning during these periods. In addition, tangential and centripetal acceleration can be calculated based on angular velocity and measured segment lengths, and then propagated along the kinematic chain (El-Gohary and McNames, 2012; Lin and Kulić, 2012; Lee and Choi, 2019).

2.2.2. Mechanisms to mitigate magnetic disturbances—Magnetic disturbances can be mitigated by considering a time-varying decay of magnetic field fluctuations (Ligorio and Sabatini, 2016). Alternatively, magnetometer measurements can be discarded if the magnetic field strength and inclination angle (i.e. direction of magnetic field relative to gravity) are not within expected ranges at a given geographic location (Ligorio and Sabatini, 2016; Sabatini (2006); Sun et al., 2013). Threshold-based mechanisms can mitigate 'dynamic' magnetic disturbances (e.g. walking through a metal door frame), but not, however, 'quasi-static' magnetic disturbances (e.g. standing under a metal door frame), which will result in gyroscopic drift. During periods in which the gyroscope must be dead-reckoned, 'still detection' algorithms can be used to zero the gyroscope when a stationary period is observed (e.g. when angular velocities are below a defined threshold for a defined duration) (Schiefer et al., 2014). Still detection mitigates but does not eliminate gyroscopic drift since the error will continue to compound during periods of movement.

Kinematic models that incorporate measurements from multiple IMUs (e.g. (Miezal et al., 2016; El-Gohary and McNames, 2012; Zhang et al., 2011; Kok et al., 2014)) can also be used to reduce the reliance on magnetometer measurements. It should be noted that these additional mechanisms add filter complexity, resulting in the need to monitor and/or control additional operational parameters (e.g. segment lengths), higher computational costs, and tuning parameters. To our knowledge, a comprehensive comparison of the various approaches of combining IMU information with a human kinematic model has not been reported.

Given current hardware limitations, the ergonomist has several suboptimal options for mitigating measurement errors associated with magnetic disturbances. These include: (i) using the system under the assumption of a homogenous magnetic field, which requires visual inspection (Robert-Lachaine et al., 2019) or other mechanisms (e.g. machine learning) (Lebel et al., 2016) to identify and discard magnetically disturbed data segments; (ii) capture data in relatively short timeframes (minutes) relative to a known orientation by dead-reckoning the IMU (Schiefer et al., 2014; El-Gohary and McNames, 2015); or (iii) use IMUs as inclinometers (Schall et al., 2016a; Kersten and Fethke, 2019; Granzow et al., 2018; Schall et al., 2014, 2016b; Yang et al., 2017). While using IMUs as inclinometers does not provide 3D measurements, more accurate postural summary metrics have been reported in comparison to accelerometer-only approaches, particularly under high motion

speeds (Chen et al., 2018). This option was explored in our previous paper, in which peak errors >25° for accelerometer-based measurement of upper arm elevation were substantially reduced (to <3°) through the use of a sensor fusion algorithm (Chen et al., 2018).

What remains unknown from our previous work, however, is whether the increased accuracy observed was a function of sensor fusion approach, differences in filter implementation, the use of a more complex gyroscope model, the inclusion of a motion mitigation mechanism, or some combination of these factors. Furthermore, we have since simplified our complementary filter design and modified it to account for gyroscope bias. Therefore, in the current paper, we evaluate four new sensor fusion algorithms, two complementary filters and two Kalman filters, that either account for gyroscope bias or not while controlling for filter implementation differences. The study objectives were to (i) improve upon our previous complementary filter design, and to (ii) evaluate the effects of sensor fusion approach and gyroscope model on the accuracy of upper arm elevation measurements.

3. Methods

3.1. Complementary filter

The complementary filter we previously developed (Chen et al., 2018) was modified to simplify its equations and extended to account for gyroscope bias. The new filter design is analogous to the work of (Gallagher et al., 2004). Gyroscope bias was considered according to (Madgwick et al., 2011).

The structure of the modified complementary filter (without accounting for gyroscope bias) is as follows:

$$\overrightarrow{g}_k = (1-\beta)\left(\overrightarrow{g}_{k-1} + \overrightarrow{g}_k \times \overrightarrow{\omega}_k \Delta t\right) + \beta \overrightarrow{a}_k \quad (1)$$

where $\overrightarrow{g}$ is the direction of the gravity estimated by the sensor fusion algorithm in the body frame, $\overrightarrow{\omega}$ is the angular velocity (rad/s) measured by the gyroscope, $\overrightarrow{a}$ is the linear acceleration (m/s^2) measured by the accelerometer, Δt is the sample period (i.e., the inverse of the sampling rate), and × is the cross product at the k and $k-1$ iterations. Since the output of this filter implementation is a 'filtered' gravitation vector, its unit is also in terms of linear acceleration (m/s^2). $\overrightarrow{g}$ is subsequently used to calculate upper arm elevation. The filter is tuned by assigning the parameter β a value between 0 and 1, where a value of 0 indicates that the filter is using solely gyroscope measurements and a value of 1 indicates that the filter is using solely accelerometer measurements. This filter will be referred to as *comp* hereafter. β was set to 0.006, which was determined experimentally.

The extended complementary filter that accounts for gyroscope bias $\overrightarrow{b}$ is presented as Equation (2):

$$\overrightarrow{g}_k = (1-\beta)\left(\overrightarrow{g}_{k-1} + \overrightarrow{g}_{k-1} \times \left(\overrightarrow{\omega}_k - \overrightarrow{b}_{k-1}\right)\Delta t\right) + \beta \overrightarrow{a}_k \quad (2)$$

$\overrightarrow{b}$ is calculated as follows:

$$\vec{b}_k = \vec{b}_{k-1} - \gamma(1-\beta)\left(\vec{g}_k \times \left(\vec{g}_k - \vec{a}_k\right)\right)\Delta t \tag{3}$$

where γ is the bias tuning parameter. A value of 0 means that gyroscope bias is unaccounted for in the model. This filter will be referred to as *comp-bias* hereafter. The filter parameter β was set to 0.003 and the parameter γ was set to 1×10^{-5}. These parameters were derived experimentally.

3.2. Kalman Filter

The process and measurement model for the Kalman Filter analogue of (1) is as follows:

$$\vec{g}_k = \left[I - \left[\vec{\omega}_{k-1}\times\right]\Delta t\right]\vec{g}_{k-1} + \left[\left[\vec{g}_{k-1}\times\right]\Delta t\right]\vec{w}_{\omega,k} \tag{4}$$

$$\vec{a}_k = \vec{g}_k + \vec{v}_{a,k} \tag{5}$$

where $[\vec{u}\times]$ is the skew symmetric operator, $\vec{w}_{\omega,k}$ is the gyroscope white noise, and $\vec{v}_{a,k}$ is the accelerometer white noise.

The process model is as follows when gyroscope bias is considered:

$$\begin{bmatrix}\vec{g}_k\\ \vec{b}_k\end{bmatrix} = \begin{bmatrix}I - \left[\left(\vec{\omega}_{k-1} - \vec{b}_k\right)\times\right]\Delta t & 0\\ 0 & I\end{bmatrix}\begin{bmatrix}\vec{g}_{k-1}\\ \vec{b}_{k-1}\end{bmatrix} + \begin{bmatrix}\left[\vec{g}_{k-1}\times\right]\Delta t & 0\\ 0 & I\Delta t\end{bmatrix}\begin{bmatrix}\vec{w}_{\omega,k}\\ \vec{b}_{\omega,k}\end{bmatrix} \tag{6}$$

where $\vec{b}_{\omega,k}$ is the gyroscope bias noise. The measurement model does not change. These are simplified versions of the filter implemented in our previous work (Chen et al., 2018).

The Kalman filter implementations without and with gyroscope bias compensation are labeled *KF* and *KF-bias*, respectively. For both, the gyroscope white noise standard deviation (SD) was set to 0.005 rad/s. For *KF*, the accelerometer noise SD was set to 0.05 m/s^2. For *KF-bias*, the gyroscope bias noise SD was set to 0.0005 rad/s^2 and the accelerometer white noise SD was set to 0.1 m/s^2. These values were derived experimentally.

3.3. Upper arm elevation calculation

Upper arm elevation θ_k in the measurement time series is calculated as follows:

$$\theta_k = \cos^{-1}\frac{g_{x,k}}{\sqrt{g_{x,k}^2 + g_{y,k}^2 + g_{z,k}^2}} \tag{7}$$

where $g_{x;k}$, $g_{y;k}$, and $g_{z;k}$ are the x, y, and z-axes of the gravity vector from the filter output at sample k. This equation assumes that the x-axis is aligned with the upper arm, with positive x oriented distally.

Upper arm angular velocity $\dot{\theta}$ is calculated as follows:

$$\dot{\theta}_k = \left| \frac{\theta_k - \theta_{k-1}}{\Delta t} \right| \quad (8)$$

3.4. Laboratory study

Participants (11 male, 3 female, mean age = 27.2 ± 6.6 years, right-hand dominant) were recruited from the University of Iowa community and screened for any self-reported cases of: (i) physician-diagnosed musculoskeletal disorders in the previous six months, (ii) pain for the previous two weeks prior to enrollment, and (iii) medical history of orthopedic surgery in the upper extremity (shoulder, elbow, wrist, hand). Each participant provided written informed consent prior to participation. The University of Iowa Institutional Review Board approved all study procedures.

An IMU (Opal, APDM, Inc. Portland, OR; also sold as series SXT, Nexgen Ergonomics, Inc., Pointe Claire, Quebec, CA) was secured to the lateral aspect of the dominant upper arm midway between the acromion and the lateral epicondyle. Accelerometer and gyroscope measurements from the IMU were recorded at a sampling rate of 128 Hz. Spatial orientation was also simultaneously recorded using a six-camera optical motion capture (OMC) system (Optitrack Flex 13, NaturalPoint, Inc., Corvallis, OR, USA) that tracked four reflective markers rigidly attached to the surface of the IMU with double-sided tape. The OMC measurements were recorded at 120 Hz. Calibration of the IMU and OMC instrumentation systems was performed using manufacturer-specified procedures. Specifically, the IMU was placed stationary on a table for >1 min to remove initial gyroscope biases using the manufacturer's software. For the OMC system, camera placement and lens distortion were determined and applied using the manufacturer's software, which associates through triangulation the position of the reflective markers registered on each camera to the known positions of reflective markers on calibration wand. A manufacturer-provided calibration square was used to define the OMC reference coordinate frame.

Each participant completed six trials of a task that required transferring wooden dowels (2 cm dia. × 8 cm length) from a waist-high container placed directly in front of the participant to a shoulder-height container placed diagonally from the participant (Fig. 3). Each participant completed two trials at each of three rates: slow (15 cycles/min), medium (30 cycles/min), and fast (45 cycles/min) dictated by a metronome. Experimental conditions were randomized to control for potential order effects. Each participant was given time to acclimate to the assigned transfer rate before each trial was captured. The trials were 1 min in duration and each was followed by a 5-min rest period. OMC measurements were recorded for the duration of each trial (1 min) while the IMU provided measurements for the entirety of each testing session (>30 min).

All post-processing was accomplished using MATLAB (2016a, Mathworks, Natick, MA). The IMU data were down sampled to 120 Hz to match the OMC sampling rate after executing the sensor fusion algorithms. For each trial, IMU and OMC measurements were temporally aligned through visual inspection. The offset between the local coordinate

frames of the OMC and the IMU was calculated using angular velocity measurements according to (de Vries et al., 2009) and subsequently applied to OMC measurements. After applying the local offset, the offset between the global coordinate frames of the OMC and the IMU was determined under static conditions using the accelerometer-derived inclination measurements. OMC-derived upper arm elevation displacements and velocities were calculated after the offsets were added to OMC-derived orientation measurements.

After alignment, the direction of gravity in the body frame was calculated from the OMC as follows

$$\begin{bmatrix} g_x \\ g_y \\ g_z \end{bmatrix} = 9.81 \begin{bmatrix} 2q_1q_3 - 2q_0q_2 \\ 2q_0q_1 + 2q_2q_3 \\ q_0^2 - q_1^2 - q_2^2 + q_3^2 \end{bmatrix} \quad (9)$$

where q_0 is the scalar component of the quaternion orientation vector and q_1, q_2, q_3 are the vector components of the quaternion orientation vector.

Root-mean-square error (RMS) for upper arm elevation was calculated as follows:

$$\theta_{err} = \sqrt{\frac{1}{n}\sum(\theta_{omc} - \theta_{imu})^2} \quad (10)$$

where θ_{omc} and θ_{imu} are the upper arm elevation measurements from the OMC and IMU, respectively. Peak error was calculated using the 99th percentile measurement of the rectified (absolute value) sample-to-sample difference between the OMC and inclinometer-derived measurements.

Similarly, RMS for upper arm angular velocity was calculated as follows:

$$\dot{\theta}_{err} = \sqrt{\frac{1}{n}\sum(\dot{\theta}_{omc} - \dot{\theta}_{imu})^2} \quad (11)$$

where $\dot{\theta}_{omc}$ and $\dot{\theta}_{imu}$ are the upper arm angular velocity measurements from the OMC and IMU, respectively. Peak error was calculated using the 99th percentile measurement of the rectified (absolute value) sample-to-sample difference between the OMC and inclinometer-derived measurements.

4. Results

Our four sensor fusion algorithms produced average and peak displacement errors of <2.5° and <4.5°, respectively, across all transfer rates. As expected, the measurement error increased marginally with increased transfer rates (<0.5° average, <1.5° peak between the 'slow' and fast' transfer rates). For each transfer rate, the difference in peak error between the Complementary and Kalman-based sensor fusion approaches differed by < 1°. The inclusion of gyroscope bias reduced peak errors by approximately 1.5° (Table 1).

Similar effects were observed for angular velocities. Errors increased with transfer rates. Peak velocity errors were <37.5°/s across all transfer rates and sensor fusion algorithms. The

Kalman Filter reduced velocity errors to a lesser extent than inclusion of bias estimation. The angular velocity errors from the complementary and Kalman Filter approaches were less than 37.2°/s and 36.3°/s, respectively. When compensation for gyroscope bias, the errors were less than 25.2°/s and 23.3°/s, respectively (Table 2).

5. Discussion

5.1. IMU error magnitudes

The observed error magnitudes (<2.5° average error across all algorithms and transfer rates) are among the lowest reported to date. The best-performing algorithm (*KF-bias*) produced average errors ≤1.2° across all transfer rates which, to our knowledge, is the lowest error reported in the literature. This is in contrast to studies that have reported errors between OMC and IMU-based orientation measures ranging from 20° to 40° (Robert-Lachaine et al., 2016; Godwin et al., 2009). To better understand the variability in reported findings, it is important to discuss methods used to assess the accuracy of IMUs, which can vary widely.

In general, the accuracy of an IMU is assessed by simultaneously measuring a motion pattern with the sensor and a reference device. An OMC system is generally used as the “gold-standard” reference for this application (Cuesta-Vargas et al., 2010). However, mechanical gimbals (Lebel et al., 2013; Lebel et al., 2015), robotic arms (El-Gohary and McNames, 2015; Martori et al., 2013; Mourcou et al., 2015), pendulums (Godwin et al., 2009; Brodie et al., 2008), and human motion (Robert-Lachaine et al., 2017; Bergamini et al., 2014; Schall et al., 2016b; Faber et al., 2013; Ligorio et al., 2016; Kim and Nussbaum, 2013; Schall et al., 2015a) have also been used as motion sources. The advantage of mechanical devices (e.g. gimbals, robotic arms) is a highly repeatable motion pattern. However, the motion dynamics (e.g. linear acceleration, angular velocities) may not be representative of human motion. Linear acceleration magnitudes below the expected magnitudes during human motion will likely result in lower IMU errors than would be anticipated when human motion is involved. Additionally, the motors on mechanical devices may provide a source of magnetic disturbance.

When IMU accuracy is evaluated using human motion, a wider range of reported errors is anticipated. A common approach, for example, is to assess IMU accuracy in the context of biomechanics (i.e. joint kinematics) (Sers et al., 2020; Plamondon et al., 2007; El-Gohary and McNames, 2012; Martori et al., 2013; Kim and Nussbaum, 2013; Schall et al., 2015a, 2015b). For this approach, joint angles calculated using a kinematic model based on measurements from an OMC system are compared to joint angles calculated using a kinematic model based on measurements from IMUs. A comparison of this type is representative of the use of IMUs for occupational exposure assessment applications. However, the variation in error magnitudes reported in studies assessing the accuracy of IMUs in this manner may reflect differences in methodology rather than sensor error (Robert-Lachaine et al., 2016). For example, when using an OMC system, the position and orientation of joint segments are typically defined based on the spatial positions of established anatomical landmarks (Wu et al., 2005). Because IMUs do not measure spatial position, joint coordinate frames cannot be defined in the same manner as the OMC system (de Vries et al., 2010). While a calibration fixture can be used to align the orientation

of an IMU relative to anatomical landmarks (Picerno et al., 2008), the common approach of aligning IMUs to joint segments entails a functional calibration procedure using pre-defined motions (Ricci et al., 2014; Favre et al., 2009; Bouvier et al., 2015). Differences in calibration procedures can lead to discrepancies ranging from 15° to 40° relative to established clinical protocols (Robert-Lachaine et al., 2016; de Vries et al., 2010; Ricci et al., 2014; Cutti et al., 2007). Soft tissue artifacts (e.g. reflective markers moving differently relative to the IMU) as well as the compounding errors of multiple IMUs, may contribute to larger error magnitudes. For these reasons, several studies report accuracy in terms of sensor error to control for methodological differences (Lebel et al., 2013; Lebel et al., 2015; Bergamini et al., 2014; Chen et al., 2018; Faber et al., 2013; Ligorio et al., 2016).

The errors associated with IMU spatial orientation measurements (i. e., heading, pitch and roll angles rather than kinematic variables) are relevant for understanding IMU error characteristics and the theoretical accuracy of biomechanical-based measurements using current sensor technologies. Errors in spatial orientation measurements are often presented when (i) developing and comparing sensor fusion algorithms and (ii) assessing factors that can negatively affect IMU accuracy (Lebel et al., 2013; Lebel et al., 2015; Bergamini et al., 2014; Ligorio et al., 2016; Sessa et al., 2012). Average sensor errors on the order of <6° have been observed (Chen et al., 2017; Lebel et al., 2013; Bergamini et al., 2014; Chen et al., 2018; Faber et al., 2013; Ricci et al., 2016). Faber et al. reported errors <1.5° (Faber et al., 2013), which is consistent with the current study findings. Variations in sensor accuracy can be attributed to how well the IMU and OMC systems were aligned both spatially and temporally (Sessa et al., 2012; Mecheri et al., 2016), the accuracy of the sensor hardware, and the performance of the sensor fusion algorithm (Chen et al., 2017). The experimental setup can also affect sensor error. A static pose (e.g., an n, T, or I-pose) followed by a short sampling timeframe (e.g. <1 min), for example, should produce minimal gyroscopic drift. When using a static positioning procedure, it is unknown whether certain algorithms can thoroughly mitigate or eliminate magnetic disturbance (e.g. (El-Gohary and McNames, 2012)) since the algorithms may perform identically to a dead-reckoned solution. Small linear acceleration magnitudes due to slow movement speeds and sensors on the trunk and proximal body segments as well as mitigation of magnetic disturbances can also minimize sensor errors. These methods result in the risk of developing a test environment that is unrepresentative of the desired operating environment for the sensors (Schiefer et al., 2014). Controlling for magnetic disturbance, for example, can be accomplished in a laboratory setting, but may be unattainable in a work environment. It should also be noted that OMC and other reference devices are also subjected to measurement errors. In particular, the OMC is designed to track the positions of reflective markers in Cartesian space. Orientation is subsequently derived from a minimum of three markers attached to the same rigid body (Yun et al., 2008; Faber et al., 2013). Consequently, the accuracy and precision of the OMC-derived orientation measurements is dependent on the spacing of the markers.

In this study, we explicitly examined upper arm elevation. As such, we did not use information from the IMU's magnetometer. Also, the linear acceleration magnitudes were lower compared to those from an IMU on the distal upper extremity. We believe, however, that the range of motion speeds chosen based on our selection of the transfer rates were representative of typical sustained motion speeds for the upper extremity. From a

technical perspective, the capability of the presented sensor fusion algorithms to mitigate displacement errors due to increased motion speeds is apparent through comparison with our previous study (Chen et al., 2018), which showed that the peak displacement error for accelerometer-derived upper arm elevation measurements exceeded 25° under the 'fast' transfer rate. The simplest of the sensor fusion algorithms presented in this paper (complementary filter without bias compensation) produced peak displacement errors <4.5° for upper arm elevation across all motion speeds. In comparison, the two complementary filter implementations in our previous paper produced peak errors of <6.5° ('Comp-1') and <5.7° ('Comp-2'). The discrepancy in error magnitudes is likely attributed to differences in filter implementation since not all three filters accounted for gyroscope bias in the sensor model. We hypothesize that the numerical instabilities associated with Euler formulation for the 'Comp-1' algorithm and slow numerical convergence in the 'Comp-2' algorithm in our previous paper were both alleviated with the current complementary filter implementation.

Accounting for gyroscope bias within the sensor fusion algorithm reduced peak displacement errors from <4.5° to <3.0° for the complementary filter and from <4.0° to <2.6° for the Kalman Filter. This finding indicates that the improvements in accuracy associated with the Kalman Filter-based approach were marginal. We hypothesize, however, that this difference would increase when the sensors are mounted on the distal extremities, which will cause higher linear acceleration magnitudes. While the difference may, in part, be attributed to a suboptimal implementation and tuning of the Kalman-based approaches relative to the Complementary-based approaches, the proprietary embedded Kalman filter within the IMU produced peak errors <2.5° across all motion conditions (Chen et al., 2018). The 'inc-KF' filter in our previous work, which accounted for gyroscope bias, and modeled non-gravitational acceleration as a time-varying decay, produced peak errors <3.2°. This indicates that the inclusion of an additional motion mitigation method was not necessary for the arm elevations present in the laboratory study.

5.2. Study limitations

Perhaps the most important limitation of this study was that the scope of our analysis was constrained to upper arm elevation measurements. The principles discussed here, however, hold for other body segments that may be of interest (e.g., the trunk, elbow, wrist). As discussed previously, error magnitudes will likely increase for IMUs attached to distal body segments as linear acceleration magnitudes increase with distance from the axis of rotation. Additionally, accurately quantifying kinematics in all three planes of motion is likely not possible without either dead reckoning of gyroscope measurements or inclusion of magnetometer measurements. Another limitation is that our results are reported in terms of sensor error, which does not consider the methodological differences between a clinical laboratory-based OMC system and our field-based inclination measurement device. Finally, the trial duration was limited to 1 min, which limits the extent to which our results generalize to longer sampling durations. However, the desired cycle time for the 'fast' transfer rate was difficult for participants to maintain beyond 1 min during preliminary testing. Regardless, given that the IMU was recording continuously across all six experimental trials, we did not observe time-dependent error manifesting over the progression of the experimental session.

5.3. Summary and recommendations

For ergonomists considering using commercially available IMU-based motion capture systems, it is important to understand that magnetic disturbance, gyroscopic drift, soft tissue artifacts, and differences in biomechanical modeling will all contribute to measurement error relative to a gold-standard OMC system with a biomechanical-based marker set. Measurement error associated with magnetic disturbances cannot currently be eliminated without discarding the magnetometer measurements from the sensor fusion algorithm, which was the approach adopted for the current study. However, certain algorithms may be better at mitigating the effects of magnetic disturbance relative to others. Gyroscopic drift is likely to be observed during periods of time when magnetometer measurements are de-weighted or discarded. Gyroscopic drift may be further minimized through the development of new algorithms and/or higher-quality gyroscopes. In the absence of these improvements, the performance of IMU systems using magnetometers will continue to be highly dependent on the environments in which they are applied. If, however, magnetometers are not used and heading information is discarded, gyroscopic drift is eliminated. The IMU effectively functions as an inclinometer under such an approach, but with the advantage of providing more accurate metrics without being subject to errors associated with gyroscopic drift nor magnetic disturbance.

When possible, it is recommended that ergonomists capture accelerometer, gyroscope, and magnetometer measurements since algorithms (both proprietary and open source) will likely continue to improve. We also recommend inspecting the data to ensure that gyroscopic drift and/or magnetic disturbance is identified in the raw sensor data before calculating kinematic information of interest. This can be accomplished through simple visual inspection, or possibly advanced machine learning approaches (Robert-Lachaine et al., 2019; Lebel et al., 2016).

For practitioners interested in using open-source algorithms, we believe that choosing application-specific algorithms will provide better measurement accuracy along with known error characteristics and failure modes. When a full 3D orientation solution is required (e.g., joint angles of the distal extremities), using an algorithm that does not reject magnetic disturbance and careful visual inspection of data segments that may be subject to magnetic disturbance should lead to improved measurement accuracy. In the event that an inclination measurement (e.g. upper arm elevation, trunk flexion/extension and lateral bending) is sufficient, using a sensor fusion algorithm such as those presented here should help avoid underestimation of exposure, in particular when needing to identify/quantify the ‘most extreme’ postures when motion speeds are ‘fast.’ For this purpose, any of the algorithms we presented, as well as other widely available algorithms (e.g. (Madgwick et al., 2011; Kok and Schön, 2019)), would likely be sufficient. The improved accuracy resulting from inclusion of additional motion mitigation mechanisms, gyroscope modeling, and more accurate estimation methods would likely be minimal.

For validation of IMU-based motion capture systems, it is recommended that sensor and biomechanical errors are reported to inform other researchers and practitioners of their error sources (Robert-Lachaine et al., 2017; Robert-Lachaine et al., 2016). Repeatable protocols on how to align IMUs to various body segments would be beneficial for

consistent use of IMUs among the ergonomics community. With regards to improving sensor fusion algorithms, new methods to identify and mitigate magnetic disturbances is an important area for continued research. This may entail leveraging kinematic models that include measurements from multiple IMUs (e.g. (Miezal et al., 2016; El-Gohary and McNames, 2012; Zhang et al., 2011; Kok et al., 2014)). It is hypothesized that incorporating kinematic models that integrate measurements from multiple IMUs (e.g. (Miezal et al., 2016; El-Gohary and McNames, 2012; Zhang et al., 2011; Kok et al., 2014)) into a single over-arching sensor fusion algorithm may be used to reduce the reliance of magnetometer measurements.

Acknowledgements

This study was supported by research funding from the Centers for Disease Control (CDC)/National Institute for Occupational Safety and Health (NIOSH). This included funding from the Heartland Center for Occupational Health and Safety at the University of Iowa (T42OH008491), the Deep South Center for Occupational Health and Safety at the University of Alabama-Birmingham (UAB) and Auburn University (T42OH008436), and a Mentored Research Scientist Development Award (K01OH011183). The findings and conclusions in this report are those of the authors and do not necessarily represent the views of the CDC/NIOSH.

Source code

The sensor fusion algorithms discussed in this paper are available at the following address: https://github.com/how-chen/imu-inclination.git.

Other code within the repository are freely available but may be in varying stages of development.

References

Bachmann ER, Yun X, Peterson CW, Apr. 2004. An investigation of the effects of magnetic variations on inertial/magnetic orientation sensors," in 2004 IEEE international conference on robotics and automation. In: 2004. Proceedings. ICRA '04, vol. 2, pp. 1115–1122. 10.1109/ROBOT.2004.1307974.

Bergamini E, Ligorio G, Summa A, Vannozzi G, Cappozzo A, Sabatini AM, Oct. 2014. Estimating orientation using magnetic and inertial sensors and different sensor fusion approaches: accuracy assessment in manual and locomotion tasks. Sensors 14 (10), 18625–18649. 10.3390/s141018625. [PubMed: 25302810]

Blair S, Duthie G, Robertson S, Hopkins W, Ball K, May 2018. Concurrent validation of an inertial measurement system to quantify kicking biomechanics in four football codes. J. Biomech 73, 24–32. 10.1016/j.jbiomech.2018.03.031. [PubMed: 29602475]

Bouvier B, Duprey S, Claudon L, Dumas R, Savescu A, Jul. 2015. Upper limb kinematics using inertial and magnetic sensors: comparison of sensor-to-segment calibrations. Sensors 15 (8), 18813–18833. 10.3390/s150818813. [PubMed: 26263993]

Brigante CMN, Abbate N, Basile A, Faulisi AC, Sessa S, Aug. 2011. Towards miniaturization of a MEMS-based wearable motion capture system. IEEE Trans. Ind. Electron 58 (8), 3234–3241. 10.1109/TIE.2011.2148671.

Brodie M.a., Walmsley A, Page W, Jun. 2008. Dynamic accuracy of inertial measurement units during simple pendulum motion. Comput. Methods Biomech. Biomed. Eng 11 (3), 235–242. 10.1080/10255840802125526.

Chang HTT, Cheng LWA, Chang JYJ, Nov. 2016. "Development of IMU-based angle measurement system for finger rehabilitation. In: 2016 23rd International Conference on Mechatronics and Machine Vision in Practice (M2VIP), pp. 1–6. 10.1109/M2VIP.2016.7827295.

Chen H, Schall MC, Fethke N, Sep. 2017. Effects of movement speed and magnetic disturbance on the accuracy of inertial measurement units. Proc. Hum. Factors Ergon. Soc. Annu. Meet 61 (1), 1046–1050. 10.1177/1541931213601745.

Chen H, Schall MC, Fethke N, Feb. 2018. Accuracy of angular displacements and velocities from inertial-based inclinometers. Appl. Ergon 67 (Suppl. C), 151–161. 10.1016/j.apergo.2017.09.007. [PubMed: 29122186]

Cloete T, Scheffer C, Aug. 2008. Benchmarking of a full-body inertial motion capture system for clinical gait analysis. In: 2008 30th Annual International Conference of the IEEE Engineering in Medicine and Biology Society, pp. 4579–4582. 10.1109/IEMBS.2008.4650232.

Cuesta-Vargas AI, Galán-Mercant A, Williams JM, Dec. 2010. The use of inertial sensors system for human motion analysis. Phys. Ther. Rev 15 (6), 462–473. 10.1179/1743288X11Y.0000000006. [PubMed: 23565045]

Cutti AG, Giovanardi A, Rocchi L, Davalli A, Sacchetti R, Dec. 2007. Ambulatory measurement of shoulder and elbow kinematics through inertial and magnetic sensors. Med. Biol. Eng. Comput 46 (2), 169–178. 10.1007/s11517-007-0296-5. [PubMed: 18087742]

de Vries WHK, Veeger HEJ, Baten CTM, van der Helm FCT, Jun. 2009. Magnetic distortion in motion labs, Implications for validating inertial magnetic sensors. Gait Posture 29 (4), 535–541. 10.1016/j.gaitpost.2008.12.004. [PubMed: 19150239]

de Vries WHK, Veeger HEJ, Cutti AG, Baten C, van der Helm FCT, Jul. 2010. Functionally interpretable local coordinate systems for the upper extremity using inertial & magnetic measurement systems. J. Biomech 43 (10), 1983–1988. 10.1016/j.jbiomech.2010.03.007. [PubMed: 20382385]

Del Rosario MB, Khamis H, Ngo P, Lovell NH, Redmond SJ, Nov. 2018. Computationally efficient adaptive error-state Kalman filter for attitude estimation. IEEE Sensor. J 18 (22), 9332–9342. 10.1109/JSEN.2018.2864989.

Douphrate DI, Fethke NB, Nonnenmann MW, Rosecrance JC, Reynolds SJ, May 2012. Full shift arm inclinometry among dairy parlor workers: a feasibility study in a challenging work environment. Appl. Ergon 43 (3), 604–613. 10.1016/j.apergo.2011.09.007. [PubMed: 22019358]

El-Gohary M, McNames J, Sep. 2012. Shoulder and elbow joint angle tracking with inertial sensors. IEEE (Inst. Electr. Electron. Eng.) Trans. Biomed. Eng 59 (9), 2635–2641. 10.1109/TBME.2012.2208750.

El-Gohary M, McNames J, Jul. 2015. Human joint angle estimation with inertial sensors and validation with A robot arm. IEEE (Inst. Electr. Electron. Eng.) Trans. Biomed. Eng 62 (7), 1759–1767. 10.1109/TBME.2015.2403368.

Faber GS, Chang C-C, Rizun P, Dennerlein JT, Oct. 2013. A novel method for assessing the 3-D orientation accuracy of inertial/magnetic sensors. J. Biomech 46 (15), 2745–2751. 10.1016/j.jbiomech.2013.07.029. [PubMed: 24016678]

Fan B, Li Q, Liu T, Dec. 2017. How magnetic disturbance influences the attitude and heading in magnetic and inertial sensor-based orientation estimation. Sensors 18 (1), 76. 10.3390/s18010076.

Favre J, Aissaoui R, Jolles BM, de Guise JA, Aminian K, Oct. 2009. Functional calibration procedure for 3D knee joint angle description using inertial sensors. J. Biomech 42 (14), 2330–2335. 10.1016/j.jbiomech.2009.06.025. [PubMed: 19665712]

Filippeschi A, Schmitz N, Miezal M, Bleser G, Ruffaldi E, Stricker D, Jun. 2017. Survey of motion tracking methods based on inertial sensors: a focus on upper limb human motion. Sensors 17 (6), 1257. 10.3390/s17061257.

Gallagher A, Matsuoka Y, Ang W-T, Sep. 2004. An efficient real-time human posture tracking algorithm using low-cost inertial and magnetic sensors. In: 2004 IEEE/RSJ International Conference on Intelligent Robots and Systems (IROS) (IEEE Cat. No.04CH37566), vol. 3, pp. 2967–2972. 10.1109/IROS.2004.1389860.

Gebre-Egziabher Demoz, Elkaim Gabriel, H., David Powell J, Parkinson Bradford, W., Apr. 2006. Calibration of strapdown magnetometers in magnetic field domain. J. Aero. Eng 19 (2), 87–102. 10.1061/(ASCE)0893-1321(2006)19:2(87).

Godwin A, Agnew M, Stevenson J, Oct. 2009. Accuracy of inertial motion sensors in static, quasistatic, and complex dynamic motion. J. Biomech. Eng 131 (11) 10.1115/1.4000109, 114501–114501. [PubMed: 20353265]

Granzow RF, Schall MC, Smidt MF, Chen H, Fethke NB, Huangfu R, Jan. 2018. Characterizing exposure to physical risk factors among reforestation hand planters in the Southeastern United States. Appl. Ergon vol. 66, 1–8. 10.1016/j.apergo.2017.07.013. [PubMed: 28958420]

Kersten JT, Fethke NB, Feb. 2019. Radio frequency identification to measure the duration of machine-paced assembly tasks: agreement with self-reported task duration and application in variance components analyses of upper arm postures and movements recorded over multiple days. Appl. Ergon 75, 74–82. 10.1016/j.apergo.2018.09.005. [PubMed: 30509539]

Kim S, Nussbaum MA, Feb. 2013. Performance evaluation of a wearable inertial motion capture system for capturing physical exposures during manual material handling tasks. Ergonomics 56 (2), 314–326. 10.1080/00140139.2012.742932. [PubMed: 23231730]

Kim S, Nussbaum MA, Jul. 2014. An evaluation of classification algorithms for manual material handling tasks based on data obtained using wearable technologies. Ergonomics 57 (7), 1040–1051. 10.1080/00140139.2014.907450. [PubMed: 24724567]

Kok M, Schön TB, Jul. 2016. Magnetometer calibration using inertial sensors. IEEE Sensor. J 16 (14), 5679–5689. 10.1109/JSEN.2016.2569160.

Kok M, Schön TB, 2019. A fast and robust algorithm for orientation estimation using inertial sensors. IEEE Signal Process. Lett 10.1109/LSP.2019.2943995, 1–1.

Kok M, Hol JD, Schön TB, Jan. 2014. An optimization-based approach to human body motion capture using inertial sensors. IFAC Proc. Vol. 47 (3), 79–85. 10.3182/20140824-6-ZA-1003.02252.

Kortier HG, Sluiter VI, Roetenberg D, Veltink PH, 2014. Assessment of hand kinematics using inertial and magnetic sensors. J. NeuroEng. Rehabil 11, 70. 10.1186/1743-0003-11-70. [PubMed: 24746123]

Kraft Edgar, 2003. A quaternion-based unscented Kalman filter for orientation tracking. In: Proceedings of the Sixth International Conference of Information Fusion, 1. IEEE, Cairns, Queensland, Australia, pp. 47–54.

LaViola JJ, Jun. 2003. A comparison of unscented and extended Kalman filtering for estimating quaternion motion. In: American Control Conference, 2003. Proceedings of the 2003, vol. 3, pp. 2435–2440. 10.1109/ACC.2003.1243440.

Lebel K, Boissy P, Hamel M, Duval C, Nov. 2013. Inertial measures of motion for clinical biomechanics: comparative assessment of accuracy under controlled conditions - effect of velocity. PLoS One 8 (11), e79945. 10.1371/journal.pone.0079945. [PubMed: 24260324]

Lebel K, Boissy P, Hamel M, Duval C, Mar. 2015. “Inertial measures of motion for clinical biomechanics: comparative assessment of accuracy under controlled conditions – changes in accuracy over time. PLoS One 10 (3), e0118361. 10.1371/journal.pone.0118361. [PubMed: 25811838]

Lebel K, Boissy P, Nguyen H, Duval C, Jul. 2016. Autonomous quality control of joint orientation measured with inertial sensors. Sensors 16 (7), 1037. 10.3390/s16071037.

Lee JK, Choi MJ, Jan. 2019. Robust inertial measurement unit-based attitude determination Kalman filter for Kinematically constrained links. Sensors 19 (4), 768. 10.3390/s19040768.

Lee JK, Park EJ, Robinovitch SN, Aug. 2012. Estimation of attitude and external acceleration using inertial sensor measurement during various dynamic conditions. IEEE Trans. Instrument. Meas 61 (8), 2262–2273. 10.1109/TIM.2012.2187245.

Ligorio G, Sabatini AM, Sep. 2015a. A linear Kalman Filtering-based approach for 3D orientation estimation from Magnetic/Inertial sensors. In: 2015 IEEE International Conference on Multisensor Fusion and Integration for Intelligent Systems (MFI), pp. 77–82. 10.1109/MFI.2015.7295749.

Ligorio G, Sabatini AM, 2015b. A novel Kalman filter for human motion tracking with an inertial-based dynamic inclinometer. IEEE (Inst. Electr. Electron. Eng.) Trans. Biomed. Eng 62 (8), 2033–2043. 10.1109/TBME.2015.2411431.

Ligorio G, Bergamini E, Pasciuto I, Vannozzi G, Cappozzo A, Sabatini AM, Jan. 2016. Assessing the performance of sensor fusion methods: application to magnetic-inertial-based human body tracking. Sensors 16 (2), 153. 10.3390/s16020153. [PubMed: 26821027]

Ligorio G, Sabatini AM, Mar. 2016. Dealing with magnetic disturbances in human motion capture: a survey of techniques. Micromachines 7 (3), 43. 10.3390/mi7030043.

Lin JFS, Kulić D, 2012. Human pose recovery using wireless inertial measurement units. Physiol. Meas 33 (12), 2099. 10.1088/0967-3334/33/12/2099. [PubMed: 23174667]

Luinge HJ, Veltink PPH, Apr. 2005. Measuring orientation of human body segments using miniature gyroscopes and accelerometers. Med. Biol. Eng. Comput 43 (2), 273–282. 10.1007/BF02345966. [PubMed: 15865139]

Madgwick SOH, Harrison AJL, Vaidyanathan R, Jun. 2011. Estimation of IMU and MARG orientation using a gradient descent algorithm. In: 2011 IEEE International Conference on Rehabilitation Robotics, pp. 1–7. 10.1109/ICORR.2011.5975346.

Martori AL, Carey SL, Alqasemi R, Ashley D, Dubey RV, Nov. 2013. Characterizing suitability of wearable sensors for movement analysis using a programmed robotic motion. In: Proceedings of the ASME 2013 International Mechanical Engineering Congress and Exposition IMECE2013, San Diego, California, USA. 10.1115/IMECE2013-65064. V01AT20A032–V01AT20A032.

Mecheri H, Robert-Lachaine X, Larue C, Plamondon A, Jun. 2016. Evaluation of eight methods for aligning orientation of two coordinate systems. J. Biomech. Eng 138 (8) 10.1115/1.4033719, 084501–084501.

Miezal M, Taetz B, Bleser G, Jul. 2016. On inertial body tracking in the presence of model calibration errors. Sensors 16 (7), 1132. 10.3390/s16071132.

Mourcou Q, Fleury A, Franco C, Klopcic F, Vuillerme N, Sep. 2015. Performance evaluation of smartphone inertial sensors measurement for range of motion. Sensors 15 (9), 23168–23187. 10.3390/s150923168. [PubMed: 26389900]

Nez A, et al. , Oct. 2018. Identification of noise covariance matrices to improve orientation estimation by Kalman filter. Sensors 18 (10), 3490. 10.3390/s18103490.

Picerno P, Cereatti A, Cappozzo A, Nov. 2008. Joint kinematics estimate using wearable inertial and magnetic sensing modules. Gait Posture 28 (4), 588–595. 10.1016/j.gaitpost.2008.04.003. [PubMed: 18502130]

Plamondon A, et al. , Nov. 2007. Evaluation of a hybrid system for three-dimensional measurement of trunk posture in motion. Appl. Ergon 38 (6), 697–712. 10.1016/j.apergo.2006.12.006. [PubMed: 17382283]

Ricci L, Taffoni F, Formica D, Sep. 2016. On the orientation error of IMU: investigating static and dynamic accuracy targeting human motion. PLoS One 11 (9), e0161940. 10.1371/journal.pone.0161940. [PubMed: 27612100]

Ricci L, et al. , Jan. 2014. A new calibration methodology for thorax and upper limbs motion capture in children using magneto and inertial sensors. Sensors 14 (1), 1057–1072. 10.3390/s140101057. [PubMed: 24412901]

Robert-Lachaine X, Mecheri H, Larue C, Plamondon A, Jul. 2016. Validation of inertial measurement units with an optoelectronic system for whole-body motion analysis. Med. Biol. Eng. Comput 1–11. 10.1007/s11517-016-1537-2.

Robert-Lachaine X, Mecheri H, Larue C, Plamondon A, Sep. 2017. Effect of local magnetic field disturbances on inertial measurement units accuracy. Appl. Ergon 63 (Suppl. C), 123–132. 10.1016/j.apergo.2017.04.011. [PubMed: 28502401]

Robert-Lachaine X, et al. , May 2019. Feasibility of quantifying the physical exposure of materials handlers in the workplace with magnetic and inertial measurement units. Ergonomics 1–10. 10.1080/00140139.2019.1612941 vol. 0, no. 0.

Roetenberg D, Luinge Henk J., Baten CTM, Veltink PH, Sep. 2005. Compensation of magnetic disturbances improves inertial and magnetic sensing of human body segment orientation. IEEE Trans. Neural Syst. Rehabil. Eng 13 (3), 395–405. 10.1109/TNSRE.2005.847353. [PubMed: 16200762]

Sabatini AM, Jul. 2006. Quaternion-based extended Kalman filter for determining orientation by inertial and magnetic sensing. IEEE (Inst. Electr. Electron. Eng.) Trans. Biomed. Eng 53 (7), 1346–1356. 10.1109/TBME.2006.875664.

Sabatini AM, Jan. 2011. Estimating three-dimensional orientation of human body parts by inertial/magnetic sensing. Sensors 11 (2), 1489–1525. 10.3390/s110201489. [PubMed: 22319365]

Schall MC Jr., Fethke NB, Chen H, Kitzmann AS, Apr. 2014. A comparison of examination equipment used during common clinical ophthalmologic tasks. IIE Trans. Occup. Ergon. Human Fact 2 (2), 105–117. 10.1080/21577323.2014.964812.

Schall MC Jr., Fethke NB, Chen H, Gerr F, May 2015. A comparison of instrumentation methods to estimate thoracolumbar motion in field-based occupational studies. Appl. Ergon 48, 224–231. 10.1016/j.apergo.2014.12.005. [PubMed: 25683549]

Schall MC, Fethke NB, Chen H, Oyama S, Douphrate DI, Aug. 2015b. Accuracy and repeatability of an inertial measurement unit system for field-based occupational studies. Ergonomics 1–12. 10.1080/00140139.2015.1079335.

Schall MC Jr., Fethke NB, Chen H, May 2016. Working postures and physical activity among registered nurses. Appl. Ergon 54, 243–250. 10.1016/j.apergo.2016.01.008. [PubMed: 26851483]

Schall MC Jr., Fethke NB, Chen H, Oyama S, Douphrate DI, Apr. 2016b. Accuracy and repeatability of an inertial measurement unit system for field-based occupational studies. Ergonomics 59 (4), 591–602. 10.1080/00140139.2015.1079335. [PubMed: 26256753]

Schiefer C, et al. , Nov. 2014. Optimization of inertial sensor-based motion capturing for magnetically distorted field applications. J. Biomech. Eng 136 (12) 10.1115/1.4028822, 121008–121008. [PubMed: 25321344]

Sers R, Forrester S, Moss E, Ward S, Ma J, Zecca M, Jan. 2020. Validity of the Perception Neuron inertial motion capture system for upper body motion analysis. Measurement 149, 107024. 10.1016/j.measurement.2019.107024.

Sessa S, Zecca M, Lin Z, Bartolomeo L, Ishii H, Takanishi A, Sep. 2012. A methodology for the performance evaluation of inertial measurement units. J. Intell. Rob. Syst 71 (2), 143–157. 10.1007/s10846-012-9772-8.

Sun G, Yang Y, Xie J, Garrett M, Wang C, Jul. 2013. Implementing quaternion based AHRS on a MEMS multisensor hardware platform. In: International Global Navigation Satellite Systems Society. Outrigger Gold Coast, Qld Australia.

Valenti RG, Dryanovski I, Xiao J, Aug. 2015. Keeping a good attitude: a quaternion-based orientation filter for IMUs and MARGs. Sensors 15 (8), 19302–19330. 10.3390/s150819302. [PubMed: 26258778]

Valenti RG, Dryanovski I, Xiao J, Feb. 2016. A linear Kalman filter for MARG orientation estimation using the algebraic quaternion algorithm. IEEE Trans. Instrument. Meas 65 (2), 467–481. 10.1109/TIM.2015.2498998.

Wu J, Zhou Z, Chen J, Fourati H, Li R, Sep. 2016. Fast complementary filter for attitude estimation using low-cost MARG sensors. IEEE Sensor. J 16 (18), 6997–7007. 10.1109/JSEN.2016.2589660.

Wu G, et al. , May 2005. “ISB recommendation on definitions of joint coordinate systems of various joints for the reporting of human joint motion—Part II: shoulder, elbow, wrist and hand. J. Biomech 38 (5), 981–992. 10.1016/j.jbiomech.2004.05.042. [PubMed: 15844264]

Yang L, Grooten WJA, Forsman M, Nov. 2017. An iPhone application for upper arm posture and movement measurements. Appl. Ergon 65, 492–500. 10.1016/j.apergo.2017.02.012. [PubMed: 28274467]

Yun X, Bachmann Eric R., Dec. 2006. Design, implementation, and experimental results of a quaternion-based Kalman filter for human body motion tracking. IEEE Trans. Robot 22 (6), 1216–1227. 10.1109/TRO.2006.886270.

Yun X, Bachmann Eric R., McGhee Robert B., Mar. 2008. A simplified quaternion-based algorithm for orientation estimation from Earth gravity and magnetic field measurements. IEEE Trans. Instrument. Meas 57 (3), 638–650. 10.1109/TIM.2007.911646.

Zhang ZQ, Wong WC, Wu JK, Jul. 2011. Ubiquitous human upper-limb motion estimation using wearable sensors. IEEE Trans. Inf. Technol. Biomed 15 (4), 513–521. 10.1109/TITB.2011.2159122. [PubMed: 21659035]

Zhang J-T, Novak AC, Brouwer B, Li Q, 2013. Concurrent validation of Xsens MVN measurement of lower limb joint angular kinematics. Physiol. Meas 34 (8), N63. 10.1088/0967-3334/34/8/N63. [PubMed: 23893094]

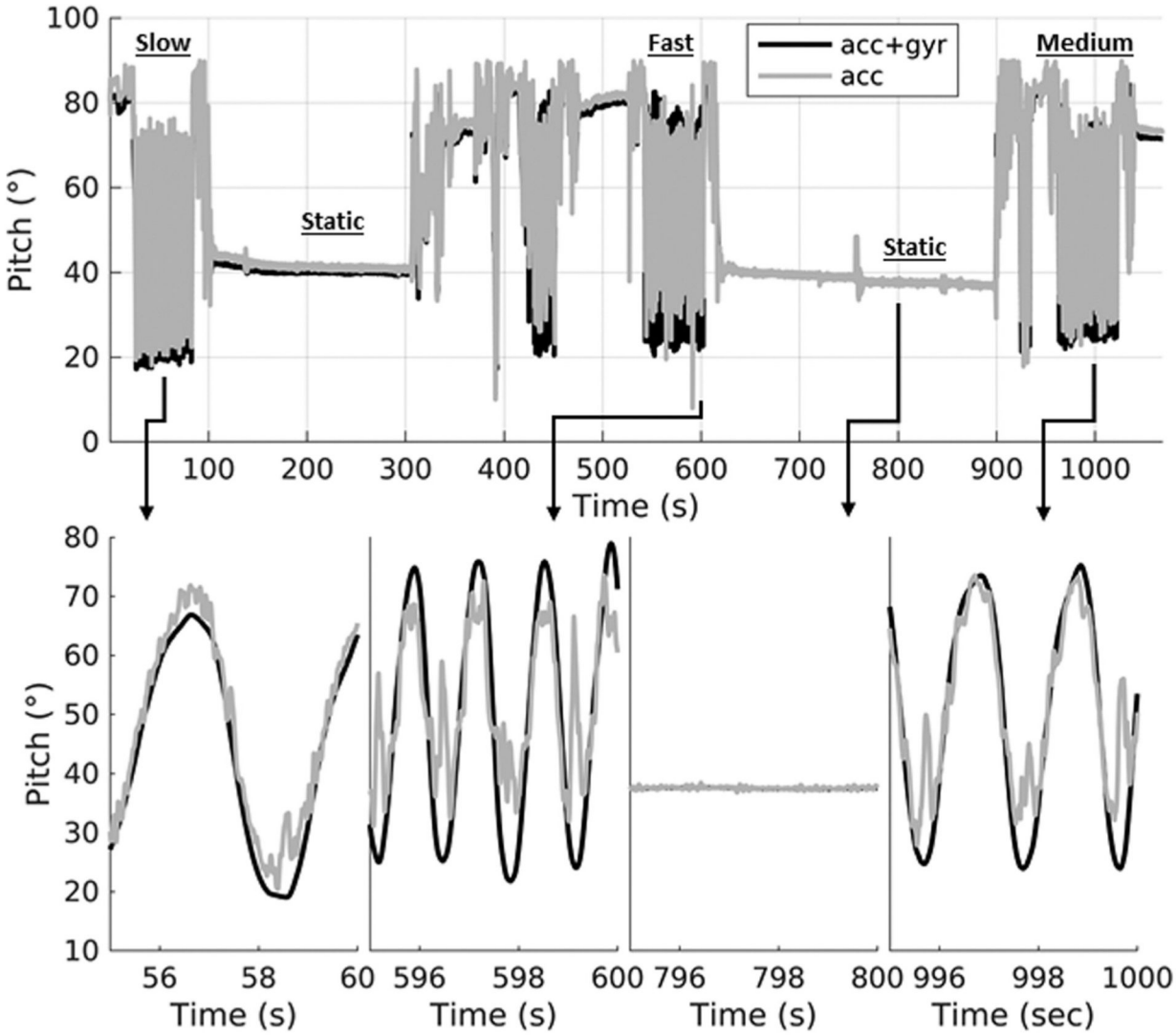

Fig. 1.

[Top:] Inclination (pitch) angles calculated using only accelerometer measurements (acc) and using a sensor fusion algorithm that combines accelerometer with gyroscope measurements (acc + gyr) under varying motion conditions (static, slow, medium, fast) across 1100 s [Bottom:] Detailed views (5-s intervals) of inclination measurements at various periods of the trial under different motion conditions.

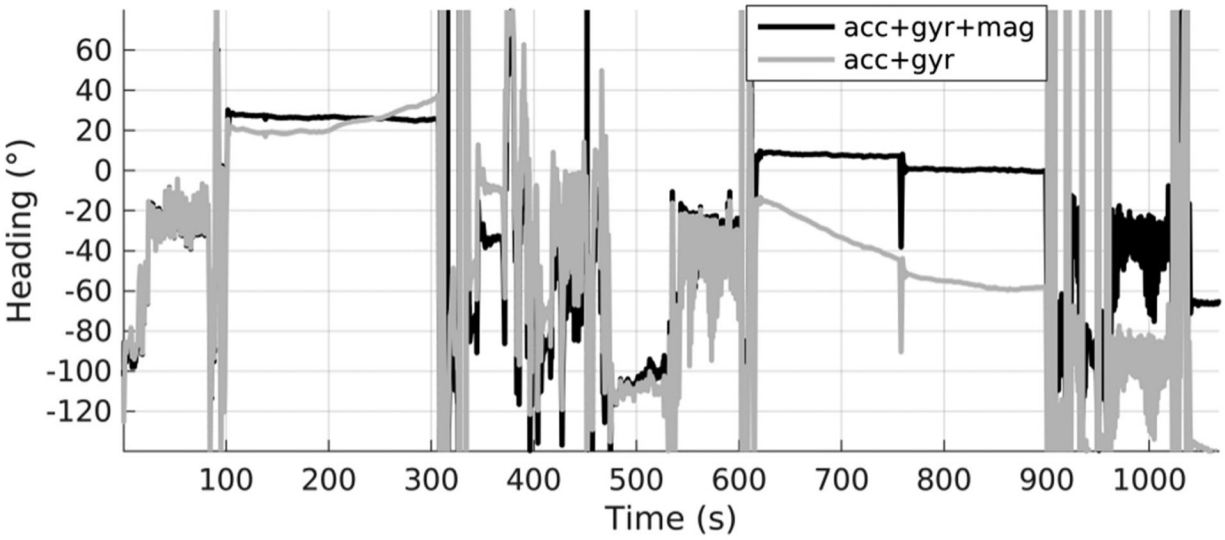

Fig. 2.

Heading (direction about gravity vector) angle calculated using a sensor fusion algorithm with magnetometer measurements (acc + gyr + mag) and without magnetometer measurements (acc + gyr).

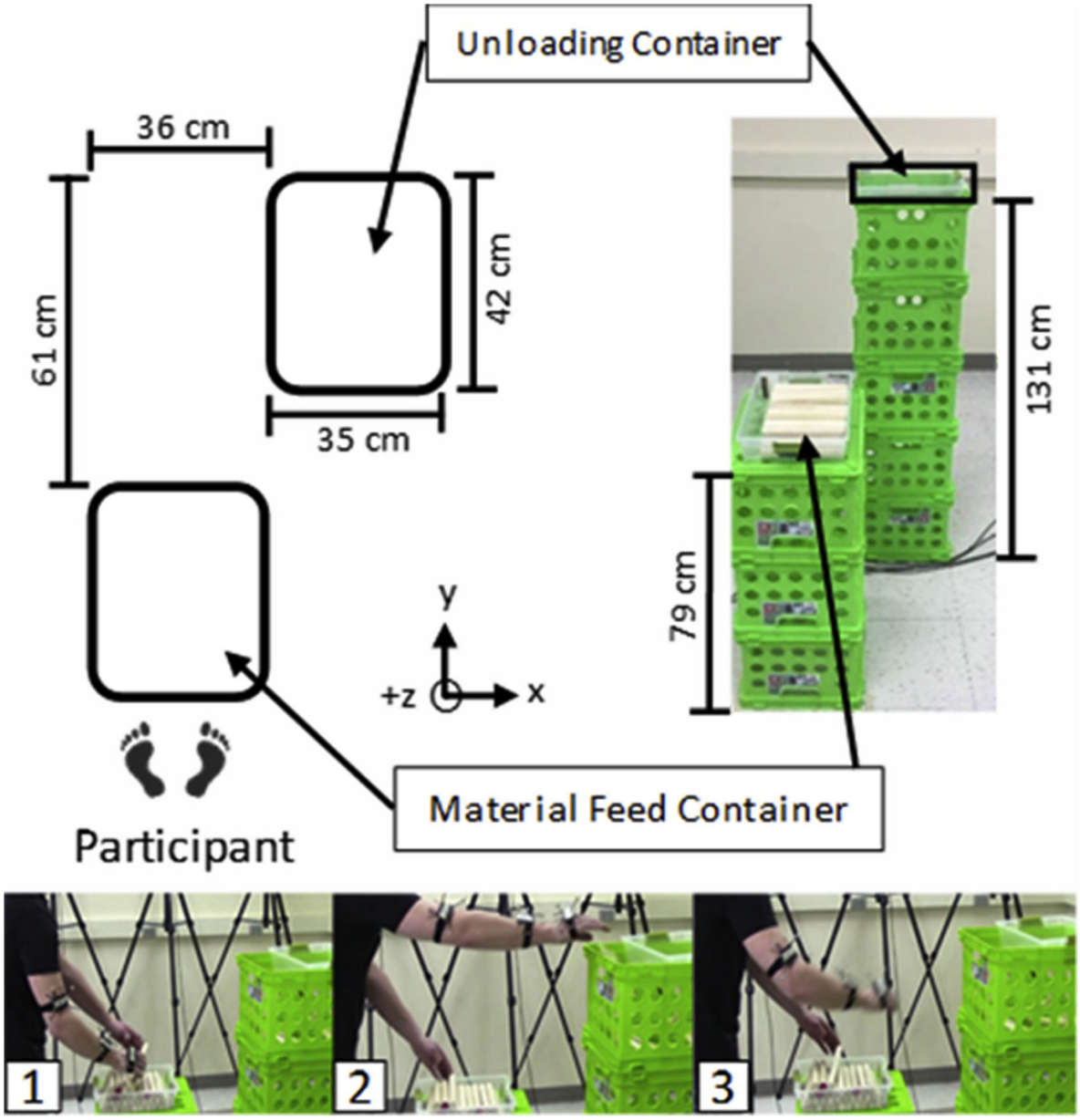

Fig. 3.

Experimental setup. Each transfer cycle consisted of (1) grasping a wooden dowel, (2) transferring the dowel to the unloading container, and (3) returning the hand back to the material feed container to grasp the next dowel.

Table 1

Mean (SD) of upper arm elevation displacement error and summary metrics across 13 participants and three material transfer rates: slow (15 cycles/min), medium (30 cycles/min), and fast (45 cycles/min) maintained for a 1-min period. Displacements were measured by the OMC system and calculated using a complementary filter without bias compensation (Comp) and with bias compensation (Comp-bias), Kalman Filter without bias compensation (KF) and with bias compensation (KF-bias). Peak error is defined as the 99th percentile of the rectified sample-to-sample difference between the OMC and IMU.

	OMC	Comp	Comp-bias	KF	KF-bias
'Slow' Transfer Rate					
RMS Error (°)	-REF-	1.9(1.4)	1.4(0.9)	1.7(1.2)	1.0(0.6)
Peak Error (°)	-REF-	3.3(2.0)	2.6(1.3)	2.9(1.8)	2.0(1.0)
Mean (°)	47.4(7.7)	47.0(8.6)	46.4(8.0)	46.9(8.5)	46.7(7.8)
10th Percentile (°)	20.5(6.4)	21.1(7.2)	20.2(6.9)	20.9(7.2)	20.4(6.6)
50th Percentile (°)	46.1(8.9)	45.4(9.6)	44.9(9.0)	45.5(9.5)	45.4(8.8)
90th Percentile (°)	75.4(8.7)	74.5(9.6)	74.0(8.9)	74.5(9.5)	74.3(8.8)
Percentile Range (90th – 10th) (°)	54.9(4.4)	53.4(4.2)	53.9(4.0)	53.6(4.2)	53.9(4.0)
Time in neutral posture (<20°) (%)	12.3(13.7)	11.5(14.2)	12.7(14.2)	11.8(14.2)	12.4(13.8)
Time in extreme posture (≥45°) (%)	50.4(7.5)	49.6(8.6)	49.3(7.9)	49.7(8.4)	49.7(7.6)
Time in extreme posture (≥60°) (%)	35.4(12.4)	34.1(13.6)	33.7(13.1)	34.2(13.5)	34.1(13.1)
'Medium' Transfer Rate					
RMS Error (°)	-REF-	2.1(1.2)	1.6(0.9)	1.9(1.1)	1.1(0.6)
Peak Error (°)	-REF-	4.0(1.8)	3.0(1.4)	3.5(1.7)	2.3(1.1)
Mean (°)	44.4(7.3)	44.0(8.1)	43.3(7.6)	44.0(8.0)	43.7(7.4)
10th Percentile (°)	19.0(6.8)	19.7(7.2)	18.6(6.9)	19.6(7.3)	19.0(6.9)
50th Percentile (°)	41.8(8.1)	41.1(8.7)	40.5(8.3)	41.1(8.6)	41.1(8.0)
90th Percentile (°)	73.1(9.1)	72.2(9.6)	71.6(9.3)	72.1(9.5)	71.8(9.0)
Percentile Range (90th – 10th) (°)	54.1(5.4)	52.5(5.2)	52.9(5.2)	52.5(5.2)	52.8(5.3)
Time in neutral posture (<20°) (%)	15.4(13.4)	14.2(14.3)	16.2(14.0)	14.3(14.3)	15.3(13.6)
Time in extreme posture (≥45°) (%)	46.3(8.5)	45.4(9.4)	44.8(8.9)	45.5(9.2)	45.5(8.7)
Time in extreme posture (≥60°) (%)	29.8(12.0)	28.3(13.2)	27.4(13.2)	28.3(13.1)	28.1(12.8)
'Fast' Transfer Rate					
RMS Error (°)	-REF-	2.4(1.3)	1.6(0.8)	2.1(1.2)	1.2(0.5)
Peak Error (°)	-REF-	4.5(1.9)	3.0(1.1)	4.0(1.7)	2.6(1.0)
Mean (°)	43.6(7.2)	43.2(8.2)	42.6(7.5)	43.2(8.1)	43.0(7.3)

	OMC	Comp	Comp-bias	KF	KF-bias
10th Percentile (°)	18.1(5.8)	18.6(6.6)	17.7(6.0)	18.6(6.6)	18.2(6.0)
50th Percentile (°)	42.3(7.9)	41.5(8.9)	41.1(8.2)	41.6(8.8)	41.7(7.9)
90th Percentile (°)	71.1(9.1)	70.3(10.0)	69.8(9.5)	70.2(9.9)	69.8(9.2)
Percentile Range (90th – 10th) (°)	53.0(6.2)	51.7(6.2)	52.1(6.2)	51.7(6.1)	51.6(6.1)
Time in neutral posture (<20°) (%)	16.1(11.4)	15.5(13.5)	17.1(12.2)	15.3(13.3)	15.9(11.8)
Time in extreme posture (≥45°) (%)	46.3(9.1)	45.4(10.4)	44.9(9.5)	45.5(10.2)	45.5(9.3)
Time in extreme posture (≥60°) (%)	28.1(12.8)	26.3(14.6)	25.6(14.2)	26.3(14.6)	26.1(13.9)

Table 2

Mean (SD) of upper arm elevation velocity error and summary metrics across 13 participants and three transfer rates: slow (15 cycles/min), medium (30 cycles/min), and fast (45 cycles/min) maintained for a 1-min period. Angular velocities were measured by the OMC system and calculated using a complementary filter without bias compensation (Comp) and with bias compensation (Comp-bias), Kalman Filter without bias compensation (KF) and with bias compensation (KF-bias). Peak error is defined as the 99th percentile of the rectified sample-to-sample difference between the OMC and IMU.

	OMC	Comp	Comp-bias	KF	KF-bias
'Slow' Transfer Rate					
RMS Error (°/s)	-REF-	4.0(1.6)	3.1(1.0)	4.0(1.4)	3.1(1.0)
Peak Error (°/s)	-REF-	12.7(5.9)	9.6(3.7)	12.9(5.2)	9.8(3.8)
Mean (°/s)	28.2(2.1)	27.6(2.1)	27.7(2.0)	27.7(2.1)	27.7(2.0)
10th Percentile (°/s)	2.6(1.1)	2.7(1.1)	2.6(1.2)	2.8(1.2)	2.7(1.2)
50th Percentile (°/s)	22.8(3.8)	22.3(3.5)	22.4(3.6)	22.4(3.4)	22.5(3.4)
90th Percentile (°/s)	61.3(8.7)	59.7(8.5)	60.1(8.4)	59.9(8.5)	60.1(8.4)
Percentile Range (90th – 10th) (°/s)	58.7(9.5)	57.0(9.2)	57.4(9.1)	57.2(9.3)	57.4(9.3)
Time at low velocities (<5°/s) (%)	19.5(6.4)	19.0(6.2)	19.4(6.4)	18.6(6.1)	19.0(6.2)
Time at high velocities (≥90°/s) (%)	1.0(1.5)	0.9(1.4)	0.9(1.4)	0.9(1.4)	0.9(1.4)
'Medium Transfer Rate					
RMS Error (°/s)	-REF-	8.2(3.6)	6.0(2.7)	7.9(2.9)	5.5(1.4)
Peak Error (°/s)	-REF-	24.9(15.3)	18.3(11.3)	24.7(12.9)	16.4(4.6)
Mean (°/s)	56.0(5.3)	54.9(5.4)	55.1(5.3)	54.9(5.4)	55.0(5.3)
10th Percentile (°/s)	7.5(2.8)	7.4(2.9)	7.4(2.8)	7.6(2.9)	7.8(2.8)
50th Percentile (°/s)	52.6(6.1)	51.3(6.0)	51.7(6.1)	51.1(5.9)	51.4(5.9)
90th Percentile (°/s)	109.7(17.3)	108.1(16.4)	108.2(16.5)	108.2(16.4)	107.7(16.8)
Percentile Range (90th – 10th) (°/s)	102.2(19.0)	100.6(17.7)	100.8(18.0)	100.6(17.8)	99.9(18.4)
Time at low velocities (<5°/s) (%)	7.9(3.8)	8.0(3.7)	8.0(3.6)	7.8(3.6)	7.6(3.7)
Time at high velocities (≥90°/s) (%)	21.7(8.5)	20.3(8.4)	20.6(8.5)	20.3(8.4)	20.2(8.7)
'Fast Transfer Rate					
RMS Error (°/s)	-REF-	12.8(4.7)	8.8(3.4)	12.2(3.9)	8.1(2.0)
Peak Error (°/s)	-REF-	37.2(20.1)	25.2(12.5)	36.3(16.2)	23.3(6.8)
Mean (°/s)	83.3(9.8)	81.8(10.1)	82.1(10.0)	81.6(10.1)	81.5(9.8)
10th Percentile (°/s)	14.5(3.1)	14.2(4.7)	14.6(4.1)	14.3(4.9)	15.1(4.0)

	OMC	Comp	Comp-bias	KF	KF-bias
50th Percentile (°/s)	86.0(10.6)	83.0(10.5)	83.8(10.6)	82.4(10.5)	82.7(10.4)
90th Percentile (°/s)	146.5(20.1)	146.4(20.0)	145.9(20.3)	146.7(20.1)	144.6(20.2)
Percentile Range (90th – 10th) (°/s)	131.9(20.2)	132.2(19.2)	131.3(20.0)	132.4(19.2)	129.4(19.9)
Time at low velocities (<5°/s) (%)	3.6(0.9)	3.9(1.3)	3.7(1.2)	3.9(1.3)	3.6(0.9)
Time at high velocities (≥90°/s) (%)	46.7(6.1)	45.0(6.3)	45.4(6.3)	44.6(6.3)	44.6(6.5)